
Article:
Solomon, SC, Liu, H-L, Marsh, DR et al. (2018) Whole Atmosphere Simulation of Anthropogenic Climate Change. Geophysical Research Letters, 45 (3). pp. 1567-1576. ISSN: 0094-8276

https://doi.org/10.1002/2017GL076950

Whole Atmosphere Simulation of Anthropogenic Climate Change

Stanley C. Solomon,[1] Han-Li Liu,[1] Daniel R. Marsh,[1] Joseph M. McInerney,[1] Liying Qian,[1] and Francis M. Vitt[1]

[1]National Center for Atmospheric Research, High Altitude Observatory, 3080 Center Green Dr., Boulder, CO 80301

Corresponding Author: Stanley C. Solomon, stans@ucar.edu

Submitted to Geophysical Research Letters, 27 December 2017
Revised, 16 January 2018

Key points

• We have performed the first comprehensive whole-atmosphere climate change simulations, including the thermosphere and ionosphere.

• Results for solar minimum conditions indicate slow warming in the troposphere, changing to rapid cooling in the upper atmosphere.

• In the mesopause region, systematic change was very small, but exhibited considerable interannual variability.

Abstract

We simulated anthropogenic global change through the entire atmosphere, including the thermosphere and ionosphere, using the Whole Atmosphere Community Climate Model - eXtended. The basic result was that even as the lower atmosphere gradually warms, the upper atmosphere rapidly cools. The simulations employed constant low solar activity conditions, to remove the effects of variable solar and geomagnetic activity. Global mean annual mean temperature increased at a rate of +0.2 K/decade at the surface and +0.4 K/decade in the upper troposphere, but decreased by about -1 K/decade in the stratosphere-mesosphere, and -2.8 K/decade in the thermosphere. Near the mesopause, temperature decreases were small compared to the interannual variation, so trends in that region are uncertain. Results were similar to previous modeling confined to specific atmospheric levels, and compared favorably with available measurements. These simulations demonstrate the ability of a single comprehensive numerical model to characterize global change throughout the atmosphere.

Plain Language Summary

We performed the first whole-atmosphere simulations of global change that include the lower atmosphere (0-15 km), middle atmosphere (15-90 km), and thermosphere-ionosphere (90-500 km). All significant known changes caused by human activity were included in a new version of the Whole Atmosphere Community Climate Model - eXtended. The basic result is that even as the lower atmosphere gradually warms, the upper atmosphere rapidly cools. Simulations were conducted using constant low solar activity conditions, in order to remove the effects of the solar cycle on the upper atmosphere. Global mean annual average temperature increased at a rate of +0.2 K/decade at the surface and +0.4 K/decade about 10 km above the surface, but decreased throughout the upper atmosphere, from about 20 km to 500 km, reaching -2.8 K/decade above 200 km. Near 90 km, very small temperature decreases were calculated, but the year-to-year variation was large, so temperature trends in that altitude region are uncertain. Results were similar to those obtained from previous work using numerical models that were confined to specific atmospheric levels, and compare favorably with available measurements. These simulations demonstrate the ability of a single comprehensive numerical model to characterize global change throughout the atmosphere.

1. Introduction

The increase of atmospheric trace gases that absorb and radiate in the infrared, primarily due to anthropogenic sources, has caused the Earth's surface and troposphere to increase in temperature, especially since the mid-1900's. Above the tropopause, however, the atmosphere has cooled, because as atmospheric density decreases with altitude, the infrared bands that enable these trace gases to absorb and emit radiation become more optically thin, and radiative cooling begins to dominate over absorption and warming. This phenomenon has been recognized since the paper by Roble and Dickinson (1989) that predicted cooling of the mesosphere and thermosphere, and earlier work that established stratospheric effects (Fels et al., 1980; Labitzke et al., 1986; Brasseur & Hitchman, 1988) and mesosphere-thermosphere cooling (Dickinson, 1984). The primary anthropogenic trace gas driving these changes is carbon dioxide (CO_2), but methane (CH_4) and chlorofluorocarbon species (CFCs) that cause depletion of stratospheric ozone (O_3) also play a role. Extensive observational work has since established the approximate rate of global temperature increase in the troposphere (e.g., Hansen et al., 2010), and estimated the temperature decreases in the upper atmosphere, as reviewed by Beig et al. (2003), Lastovicka et al. (2006, 2012, 2017), Qian et al. (2011), and references therein. The rate of upper atmosphere cooling varies considerably with altitude, and is difficult to measure in some ranges, but the evidence is most conclusive in the thermosphere, where decreases in neutral density and temperature inferred from observations of the effect of atmospheric drag on satellite orbits have shown the most dramatic climate change of any altitude region (Keating et al., 2000; Emmert et al., 2004, 2008; Marcos et al., 2005; Saunders et al., 2011), confirming the predictions by Roble and Dickinson. Subsequent modeling work in the mesosphere-thermosphere (e.g., Rishbeth & Roble, 1992; Akmaev & Fomichev, 2000; Qian et al., 2006, 2013, 2014; Akmaev, 2012; Solomon et al., 2015) and in the stratosphere-mesosphere (e.g., Akmaev et al., 2006; Garcia et al., 2007; Fomichev et al., 2007; Lübken et al., 2013) extended the analysis and clarified the mechanisms. In these model simulations, CO_2 is the dominant driver of temperature change, but CH_4, O_3, and possibly water vapor (H_2O), play significant roles in the stratosphere and mesosphere.

Together with the extensive efforts to model and measure climate change in the oceans, land masses, and troposphere, these piecewise model results present a nearly-complete description of anthropogenic climate change throughout the atmosphere. However, a comprehensive single-model simulation that extends into the thermosphere and ionosphere has not previously been attempted. Our objective in this study was to perform an integrated simulation of all atmospheric regions, that included a complete treatment of dynamics, chemistry, and radiative transfer. We used the NCAR Whole Atmosphere Community Climate Model—eXtended (WACCM-X) to examine the effects of anthropogenic global temperature change due to all known greenhouse gas emissions, including CO_2, CH_4, and CFCs. The studies were conducted for solar minimum conditions over a ~30 year time period. We compared these model simulations to the available data on secular trends as a function of altitude, and to previous work that addressed various segments of the atmosphere.

2. Model Description

WACCM-X is a global general circulation model that calculates 3D temperature, density, wind, composition, ionospheric, and electric potential fields from the surface to the exobase. It is a configuration of the NCAR Community Earth System Model (CESM) (Hurrell et al., 2013),

and thus is uniquely capable of coupling to dynamic or specified ocean, land, and ice models. WACCM-X is based on the Community Atmosphere Model (CAM) component of CESM, and incorporates the physics and chemistry of "regular" WACCM, which has an upper boundary of ~130 km, but does not include an interactive ionosphere. The thermosphere and ionosphere components of WACCM-X add major and minor neutral species composition, electron and ion density and composition, and electron and ion temperature, using methods originating with model predecessors (Roble et al., 1988; Richmond et al., 1992; Roble & Ridley, 1994). The model assumes hydrostatic equilibrium and uses a log-pressure coordinate system, with the pressure levels extending from 0 to ~600 km in altitude; the height of the upper boundary is dependent on solar activity. The simulations employed here use 1.9º × 2.5º horizontal resolution, and 0.25 scale height vertical resolution above 1 hPa. Solar ultraviolet irradiance is parameterized using proxy models or supplied by measurements (Solomon & Qian, 2005). Auroral particle precipitation, and an imposed magnetospheric electric field, are estimated using the geomagnetic *Kp* index. Gravity wave effects are parameterized based on the linear saturation theory of Lindzen (1981). In the mesosphere and lower thermosphere region, a radiative transfer algorithm for CO_2 that was developed by Fomichev et al. (1998) is employed. For the basic formulation of WACCM and WACCM-X, see Marsh et al. (2007) and Liu et al. (2010). Recent developments, resulting in the impending release of WACCM-X v. 2.0 as part of CESM v. 2.0, include an interactive low-latitude electric field and ionospheric dynamical transport, which are described in Liu et al. (2018). However, WACCM-X is currently based on CAM4 and WACCM4 physics and chemistry (Neale et al., 2013; Marsh et al., 2013), as released in CESM v. 1.0, and thus lags the new version of CESM by a generation. The simulations shown here were conducted with a pre-release trunk version of WACCM-X v. 2.0, internally designated 5.4.99. The model can be used in either a free-running climate mode, or with imposed meteorology analysis fields in the troposphere-stratosphere; see Marsh et al. (2013) for further discussion of chemistry, radiative transfer, and other forcings such as volcanic aerosols.

3. Climate Change Simulations

Simulations were conducted for perpetual solar minimum conditions, in order to eliminate the effects of solar irradiance and geomagnetic activity variation, which can be very significant above the mesopause. The approach employed was to conduct a five-year simulation for the years 1972–1976, and compare it to a five-year simulation for the years 2001–2005. The purpose of the five-year interval was to serve as a small ensemble, in order to reduce the effect of interannual variability on the ensemble means, and to estimate that variability as a function of altitude. For each case, the model was run for a year before the start of the study interval, to assure that minor chemical constituents had equilibrated. Lower boundary conditions specifying time-dependent trace gas inputs were the same as the standard reference case employed in the Chemistry Climate Model Initiative [Eyring et al., 2013], (see Table 1). Free-running climate simulations were employed, except that an empirical stratospheric quasi-biennial oscillation (QBO), and observed sea surface temperatures, were imposed. Monthly mean results were archived for all fields, and annual means of temperatures (neutral, ion, and electron), neutral density, electron density, and geopotential height, were derived. Zonal mean annual means were then calculated, and five-year zonal means obtained from the annual means. The temperature differences between the 1972–1976 runs and the 2001–2005 runs were calculated on pressure surfaces, and are shown in Figure 1 as a function of latitude and log-pressure. The approximate altitudes corresponding to the pressure surfaces are shown on the right-side axis.

Global mean annual means, and five-year averages of the global means, were calculated from the zonal means using cosine(latitude) weighting. The global mean profiles and changes for temperature and mass density are plotted in Figure 2. In Figure 2(a,b), the temperatures and density profiles are plotted with respect the global mean geometric altitude z, derived from geopotential height using the relationship $z=h/(1-h/r_E)$, to account for the variation of gravitational acceleration (where h is geopotential height, and r_E is the mean radius of the Earth) (Akmaev et al., 2010). The density change shown in Figure 2(d) is also plotted with respect to geometric altitude, with the 2001–2005 results interpolated onto the 1972–1976 altitudes. However, the temperature changes in Figure 2(c) are computed on pressure surfaces, similar to Figure 1, to avoid the misleading convolution of pressure level subsidence with cooling temperatures. The changes at key altitudes are summarized in Table 1, converted from the 29-year period between ensembles into K/decade, in order to facilitate comparison with other modeling and observational work.

Interannual variations of global mean temperatures are explored in Figure 3. This is a plot of the difference between the global mean annual mean temperature in each year, and the 1972–1976 mean. Although ten years are not enough to fully quantify interannual variations, they yield a coherent result: the model variance in this very broad parameter is modest throughout the lower and middle atmosphere, a fraction of a degree K at most, but increases to ~1 K near the mesopause. In the thermosphere, the variance remains on the order of 1 K, but becomes smaller on a percentage basis as the temperature increases, and of course is much smaller than the change induced by external solar/geomagnetic forcing, which is not included in these experiments.

4. Comparison to Previous Models and Observations

4.1 Troposphere

Since the sea surface temperatures used in these model runs were specified from measurements, model results for the lower troposphere are strongly influenced by this boundary condition, and no significant departure from the observed global temperature variation is expected. The modeled global average temperature change from 1972–1976 to 2001–2005 increases with altitude from ~ +0.2 K/decade at the surface to ~ +0.4 K/decade at ~10 km (266 hPa). Corresponding surface changes are ~ +0.15 K in the NCAR sea surface temperature analysis (Huang et al., 2015, 2017) and ~ +0.2 K/decade in the GISS land-sea temperature record (Hansen et al., 2010). This is in accord with various climate models as summarized by Intergovernmental Panel on Climate Change reports, which yield a model consensus ~ +0.2 K/decade increase in surface temperature (IPCC, 2014). The CESM v. 1.0 (CAM5) large ensemble run (Kay et al., 2015) also obtained an average of ~ +0.2 K/decade surface temperature increase during the years 1970–2000, as did Marsh et al. (2013), using WACCM4 and a fully-coupled ocean. Garcia et al. (2007), using WACCM3, found ~ +0.15 K/decade at the surface, increasing to ~ +0.3 K/decade near 10 km altitude. Since WACCM-X is based on CAM and WACCM, it is unsurprising but reassuring that these results are in general agreement with those from other versions of the CESM.

4.2 Stratosphere

Results shown in Figures 1 and 2 exhibit a transition from tropospheric warming to -1.1 K/decade cooling at the stratopause, with the zero-crossing line just above the tropopause on a global average basis. This is similar to Garcia et al. (2007), who also found the zero-crossing

near the tropopause, and -1.4 K/decade at the stratopause. Fomichev et al. (2007), using the Canadian Middle Atmosphere Model (CMAM), estimated -10 K temperature change at the stratopause for a doubled-CO_2 scenario, which translates to ~ -1.4 K/decade, assuming that temperature change is approximately linear with CO_2 increase. Marsh et al. (2013), comparing 2005 to a pre-industrial case, found -8 K at the stratopause, which is also ~ -1.4 K/decade, under the same assumption. There is considerable structure in the zonal means, however, especially in the high-latitude southern hemisphere, with cooling in the lower stratosphere, likely due to O_3 reduction, but modulated by increasing vortex strength (Calvo et al., 2017). There is a very small temperature increase in the southern hemisphere middle stratosphere seen in Figure 1, and in Figure 5 of Garcia et al. (2007), but we agree with Garcia et al. that this is not statistically significant. Randel et al. (2017) compared global average temperature trends for 1979–1997, the period of maximum rate of O_3 depletion, to WACCM4, and found good agreement, with ~ -1 K/decade in the middle stratosphere, and agreement with measured O_3 variability and trends.

4.3 Mesosphere

The model simulations show global mean cooling throughout the mesosphere, but decreasing with altitude from -1.1 K/decade at the stratopause to -0.2 K/decade at the mesopause. This is similar to previous WACCM results (Garcia et al., 2007), earlier simulations by Akmaev and Fomichev (2000), CMAM simulations (Fomichev et al, 2007), and the Leibniz-Institute Middle Atmosphere (LIMA) model (Lübken et al., 2013). Observational evidence is reviewed by Laštovička (2017), including the results from Huang et al. (2014) showing cooling on the order of -1 K/decade in the middle mesosphere, but also reducing to nearly undetectable near the mesopause. Other observations reviewed by Laštovička, including ground-based lidar, radar, and optical measurements, yield inconsistent results near the mesopause, supporting the contention that the effects of anthropogenic change on this region of the atmosphere are still uncertain, since it is dynamically complex, and has significant interannual variation, as discussed below.

4.4 Thermosphere

The thermosphere is the region of the atmosphere subject to the largest anthropogenic changes in temperature, on an absolute basis and also on a percentage basis. These cause even larger changes in density (at constant altitude), which is the primary means of detecting and quantifying the temperature change. However, the picture is complicated by variable solar ultraviolet and geomagnetic heating, both of which are manifestations of solar activity, especially on 11-year solar cycle time scales. Nevertheless, this is where upper atmosphere global change was first detected, by Keating et al. (2000), using the simple expedient of comparing three successive solar minimum periods. Independent analyses by Emmert et al. (2004, 2008, 2015), Marcos et al. (2005), and Saunders et al. (2011), have confirmed these findings, using various methods of accounting for solar activity, but with considerable spread with regard to the magnitude of the rate of cooling. There has also been variation in the model estimates over the years, starting with the original 1D calculation by Roble and Dickinson (1989), and continuing with 3D global modeling, most recently using Thermosphere-Ionosphere-Mesosphere-Electrodynamics General Circulation Model (TIME-GCM) simulations (Qian et al., 2011, 2014; Solomon et al., 2015). For the low solar activity case, the measurements and models appear to be on a convergent path, but the dependence of the rate of change on the level of solar activity remains in doubt (Emmert, 2015) as discussed below. At any rate, there is unanimity with regard to the sign of the change, and the reality of thermospheric cooling and contraction. This is summarized in Table 1, using density change at the benchmark 400 km altitude as the metric.

There are other means of inferring neutral temperature change, including radar measurements of ion temperature T_i, which is strongly linked to neutral temperature up to the peak of the *F*-region ionosphere (hmF_2). Modeled change in T_i at hmF_2 is shown in Table 1, as well as change in hmF_2, and the peak density (NmF_2). However, there was little or no change in the peak density of the *E*-region ionosphere (*NmE*) near 110 km. Ionospheric changes are not the focus of this letter, but are reported here for comparison with the various measurement analyses. In the case of T_i, work by Zhang et al. (2011, 2013, 2016) found -10 K/decade to -30 K/decade at various locations and altitudes. These results are much larger than observational estimates based on satellite drag (cf., Akmaev, 2012).

5. Discussion

The two five-year simulations conducted for this study are equivalent to two ensembles of five one-year runs. Each of them span just over two full cycles of the QBO, and both periods happen to contain both phases of the Pacific Ocean southern oscillation. Five-year ensembles would not be sufficient for fully characterizing regional troposphere-ocean climate variability, but are sufficient for the purpose here of quantifying global mean upper atmosphere change, and estimating its interannual variation. The intervals chosen also span the most significant period of stratospheric O_3 depletion through the 1970's and 1980's, reaching a broad minimum in the late 1990's. This is important in driving stratosphere and also mesosphere change, but makes a very minor contribution to thermosphere/ionosphere change. CH_4 increase, which results in changes in middle-atmosphere water vapor and odd-hydrogen, also has little effect on the thermosphere. CO_2 remains the primary driver of anthropogenic global climate change, throughout the atmosphere, but especially in the thermosphere, as shown by Qian et al. (2013).

Observational work has yielded inconsistent results in the mesopause region, and previous modeling work has predicted little or no global mean temperature trends. This is likely due to the dominance of dynamical processes in controlling mesopause temperature, which exhibit significant interannual variability, even without variable solar forcing. The seasonal-latitudinal behavior of trends could be important, however, especially with regard to the development of polar mesospheric clouds during the summer months, but on a global mean annual mean basis, any trends developing within the past several decades would still be within the envelope of interannual variance, as seen in Figure 3. Similarly, these simulations did not identify significant change in the lower ionosphere *E*-region, although small observed trends have been reported (e.g., Bremer, 2008). Other controversial aspects of mesopause processes and trends relate to questions concerning changes in gravity waves, eddy diffusion, turbopause height, and their effects on CO_2 and atomic oxygen profiles. Recent work by Qian et al. (2017) and the analysis by Laštovička (2017) have laid to rest various speculative mechanisms in favor of the known ones: infrared cooling by molecules that are radiationally active in the infrared.

Model estimates of these radiative processes nevertheless contain considerable uncertainties, especially with regard to the collisional excitation/deactivation rates of CO_2 and nitric oxide (NO) with atomic oxygen (cf., Solomon et al., 2015). Similarly, quantifying the solar cycle effects on thermospheric density, both to remove it from trend analyses and to understand how these trends vary with the level of solar activity, remains a challenging problem. Although Emmert et al. (2008) found that thermospheric cooling is largest under solar minimum conditions and decreases with increasing solar activity, Emmert (2015) cast doubt on the statistical significance of this finding, because it now seems possible that solar ultraviolet irradiance and solar-geomagnetic activity has been systematically decreasing over the past several cycles. This

is especially a problem for solar minimum conditions, as explored by Solomon et al. (2010, 2011, 2013), which could be an issue for the original Keating et al. (2000) approach of comparing successive solar minima.

Another problem with observational evidence of thermospheric cooling is that analyses of T_i measured by ground-based radars appear to show cooling rates as much as an order of magnitude larger than those derived from satellite drag. These may also be affected by secular decline in solar activity, but interpretation of local ground-based sampling of the ionosphere can be problematical, due to secular variation of the magnetic field (e.g., Cnossen & Richmond, 2012). Regardless, a rate of change as large as -30 K/decade would cause a 50% reduction of thermospheric density over the 50-year span of radar and satellite-drag data records, which would be conspicuous in other thermosphere and ionosphere measurements, including hmF_2.

6. Conclusion

Simulations of anthropogenic change show global mean annual mean temperatures increasing in the troposphere but decreasing in the upper atmosphere, from the lower stratosphere to the exobase, with the possible exception of the mesopause region. Although this observational and theoretical fact is sometimes considered paradoxical, it is instead a demonstration of the ability of numerical models to describe the complex dynamics, chemistry, and radiative transfer that occur throughout the atmosphere. There is general agreement between observations and models of the rate of temperature change as a function of altitude, but unresolved discrepancies do remain, particularly at altitudes that are difficult to measure accurately over extended time periods, such as the mesosphere and lower thermosphere. Since there are still some criticisms concerning the observational data and modeling techniques used to characterize temperature changes near the Earth's surface, there is risk that work by the international upper-atmosphere trends community may be deliberately misconstrued as confusion concerning the mechanisms of global change. Nevertheless, whole atmosphere modeling demonstrates not only the complexity of atmospheric processes, but the success of comprehensive numerical simulations in describing them.

These simulations were conducted using perpetual solar minimum conditions, in order to eliminate the confounding effects of solar activity variation, especially in the thermosphere. Our next simulations will be for solar maximum, in order to investigate the solar cycle effect on the rate of change throughout the atmosphere. Subsequently, we will do a fully-transient run, with all time-dependent lower boundary and solar/geomagnetic forcings, and analyze the results using the same multi-variate methods used to investigate observational data sets. We will also perform simulations with a fully-coupled ocean model. These studies will better characterize the solar cycle and other dependencies, but the basic atmospheric response to anthropogenic change is revealed through the solar minimum case described here. These findings largely confirm earlier results using models describing limited atmospheric regions, but by performing simulations using a single integrated model, we demonstrate the ability of a consistent and comprehensive set of dynamics, physics, and chemistry to describe global change throughout the atmosphere.

Acknowledgments. The authors acknowledge the pioneering work by the progenitors of whole atmosphere modeling, Byron Boville, Rolando Garcia, and Ray Roble, and essential contributions by the many members of the WACCM, CAM, and CESM development teams. As a component of the Community Earth System Model, WACCM-X source code and results are publicly available at the NCAR web site. Model output data used in this letter are archived on the NCAR High Performance Storage System. This work was supported by NSF grant 1135432, and by NASA

grants NNX14AH54G, NNX15AJ24G and NNX16AB82G. NCAR is supported by the National Science Foundation.

References

Akmaev, R. A. and V. I. Fomichev (2000), A model estimate of cooling in the mesosphere and lower thermosphere due to the CO_2 increase over the last 3–4 decades, *Geophys. Res. Lett., 27*, 2113.

Akmaev, R. A., V. I. Fomichev, and X. Zhu (2006), Impact of middle-atmospheric composition changes on greenhouse cooling in the upper atmosphere. *J. Atmos. Solar-Terr. Phys., 68,* 1879-1889, doi:10.1016/j.jastp.2006.03.008.

Akmaev, R. A., F. Wu, T. J. Fuller-Rowell, H. Wang, and M. D. Iredell (2010), Midnight density and temperature maxima, and thermospheric dynamics in Whole Atmosphere Model simulations, *J. Geophys. Res.*, *115*, A08326, doi:10.1029/2010JA015651.

Akmaev, R. A. (2012), On estimation and attribution of long-term temperature trends in the thermosphere, *J. Geophys. Res., 117*, A09321, doi:10.1029/2012JA018058.

Beig, G., et al. (2003), Review of mesospheric temperature trends, *Rev. Geophys. 41*, 1015. doi:10.1029/2002RG000121.

Brasseur, G., and M. H. Hitchman (1988), Stratospheric response to trace gas perturbations—changes in ozone and temperature distributions, *Science*, *240*, 634-637, doi:10.1126/science.240.4852.634.

Bremer, J., (2008) Long-term trends in the ionospheric *E* and F_1 regions. *Ann. Geophysicae*, *26,* 1189-1197.

Calvo, N., R. R. Garcia, and D. E. Kinnison (2017), Revisiting Southern Hemisphere polar stratospheric temperature trends in WACCM: The role of dynamical forcing, *Geophys. Res. Lett.*, *44*, 3402–3410, doi:10.1002/2017GL072792.

Cnossen, I., and A. D. Richmond (2012), How changes in the tilt angle of the geomagnetic dipole affect the coupled magnetosphere-ionosphere-thermosphere system, *J. Geophys. Res.*, *117*, A10317, doi:10.1029/2012JA018056.

Dickinson, R . E. (1984), Infrared radiative cooling in the mesosphere and lower thermosphere, *J. Atmos. Terr. Phys.*, *6*, 995-1008, doi:10.1016/0021-9169(84)90006-0.

Emmert, J. T., J. M. Picone, J. L. Lean, and S. H. Knowles (2004), Global change in the thermosphere: Compelling evidence of a secular decrease in density, *J. Geophys. Res.*, *109*, A02301, doi:10.1029/2003JA010176.

Emmert, J. T., J. M. Picone, and R. R. Meier (2008), Thermospheric global average density trends 1967-2007, derived from orbits of 5000 near-Earth objects, *Geophys. Res. Lett., 35*, L05101, doi: 10.1029/2007GL032809.

Emmert, J. T. (2015), Altitude and solar activity dependence of 1967–2005 thermospheric density trends derived from orbital drag, *J. Geophys. Res. Space Physics*, *120*, doi:10.1029/2015JA021047.

Eyring, V., et al. (2013), Overview of IGAC/SPARC Chemistry-Climate Model Initiative (CCMI) community simulations in support of upcoming ozone and climate assessments, *SPARC Newsletter*, *40*, 48–66.

Fels, S. B., J. D. Mahlman, M. D. Schwarzkopf, and R. W. Sinclair (1980), Stratospheric Sensitivity to Perturbations in Ozone and Carbon Dioxide: Radiative and Dynamical Response, *J. Atmos. Sci.*, *27*, 2265-2297, doi:10.1175/1520-0469(1980)037<2265:SSTPIO> 2.0.CO;2.

Fomichev, V.I., J.-P. Blanchet, and D. S. Turner (1998), Matrix parameterization of the 15-mm CO_2 band cooling in the middle and upper atmosphere for variable CO_2 concentration. *J. Geophys. Res., 103*, 11,505.

Fomichev, V. I., A. I. Jonsson, J. de Grandpre, S. R. Beagly, C.McLandress, K. Semeniuk, and T. Shepherd (2007), Response of the middle atmosphere to CO2 doubling: Results from the Canadian middle atmosphere model, *J. Climate*, *20*, 1121–1144, doi:10.1175/JCLI4030.1.

Garcia, R. R., D. R. Marsh, D. E. Kinnison, B. A. Boville, and F. Sassi (2007), Simulation of secular trends in the middle atmosphere, 1950–2003, *J. Geophys. Res.*, *112*, D09301, doi:10.1029/2006JD007485.

Garcia, R. R., M. López-Puertas, B. Funke, D. R. Marsh, D. E. Kinnison, A. K. Smith, and F. González-Galindo (2014), On the distribution of CO_2 and CO in the mesosphere and lower thermosphere, *J. Geophys. Res. Atmos.*, *119*, doi:10.1002/2013JD021208.

Hansen, J., R. Ruedy, M. Sato, and K. Lo (2010), Global surface temperature change, *Rev. Geophys.*, *48*, RG4004, doi:10.1029/2010RG000345.

Huang, B., et al (2015), Extended reconstructed sea surface temperature version 4 (ERSST.v4), Part I: upgrades and intercomparisons, *J. Climate*, *28*, doi:10.1175/JCLI-D-14-00006.1.

Huang, B., et al (2017), The climate data guide: SST data: NOAA extended reconstruction SSTs, version 4, Retrieved from https://climatedataguide.ucar.edu/climate-data/sst-data-noaa-extended-reconstruction-ssts-version-4.

Huang, F. T., H. G. Mayr, J. M. Russell III, and M. G. Mlynczak (2014), Ozone and temperature decadal trends in the stratosphere, mesosphere and lower thermosphere, based on measurements from SABER on TIMED, Ann. Geophys., 32, 935-949, doi:10.5194/angeo-32-935-2014.

Hurrell, J. W., M. M. Holland, P. R. Gent, S. Ghan, J. E. Kay, P. J. Kushner, J.-F. Lamarque, W. G. Large, D. Lawrence, K. Lindsay, W. H. Lipscomb, M. C. Long, N. Mahowald, D. R. Marsh, R. B. Neale, P. Rasch, S. Vavrus, M. Vertenstein, D. Bader, W. D. Collins, J. J. Hack, J. Kiehl, and S. Marshall (2013), The community earth system model: A framework for collaborative research, *Bulletin of the American Meteorological Society*, *94*, 1339–1360, doi:10.1175/BAMS-D-12-00121.1.

IPCC (2014), Climate Change 2014: Synthesis Report. Contribution of Working Groups I, II and III to the Fifth Assessment Report of the Intergovernmental Panel on Climate Change [Core Writing Team, R.K. Pachauri and L.A. Meyer (eds.)]. IPCC, Geneva, Switzerland, 151 pp.

Kay, J. E., et al. (2015), A Community Resource for Studying Climate Change in the Presence of Internal Climate Variability, *Bulletin of the American Meteorological Society*, *96*, 1335, doi:10.1175/BAMS-D-13-00255.1.

Keating, G. M., R. H. Tolson, and M. S. Bradford (2000), Evidence of long-term global decline in the Earth's thermospheric densities apparently related to anthropogenic effects, *Geophys. Res. Lett.*, *27*, 1523-1526.

Labitzke, K., G. Brasseur, B. Naujokat, and A. De Rudder (1986), Long-term temperature trends in the stratosphere: Possible influence of anthropogenic gases, *Geophys. Res. Lett.*, *13*, 52-55, doi:10.1029/GL013i001p00052.

Laštovička, J., R. A. Akmaev, G. Beig, J. Bremer, and J. T. Emmert (2006), Global change in the upper atmosphere, *Science, 314*, 1253–1254.

Laštovička, J., S. C. Solomon, and L. Qian (2012), Trends in the neutral and ionized upper atmosphere, *Space Sci. Rev.*, *168*, 113, doi:10.1007/s11214-011-9799-3

Laštovička, J. (2017), A review of recent progress in trends in the upper atmosphere, *J. Atmos Solar Terr. Phys.*, *163*, 2–13, doi:0.1016/j.jastp.2017.03.009.

Lindzen, R. S. (1981), Turbulence and stress owing to gravity wave and tidal breakdown, *J. Geophys. Res., 86*, 9707-9714.

Liu, H.-L., et al. (2010), Thermosphere extension of the Whole Atmosphere Community Climate Model, *J. Geophys. Res.*, *115*, A12302, doi:10.1029/2010JA015586.

Liu, H.-L., et al. (2018), Development and validation of the Whole Atmosphere Community Climate Model with thermosphere and ionosphere extension (WACCM-X v. 2.0), *J. Adv. Mod. Earth Sys.*, *10*, doi:10.1002/2017MS001232.

Lübken, F.-J., U. Berger, and G. Baumgarten (2013), Temperature trends in the midlatitude summer mesosphere, *J. Geophys. Res. Atmos.*, *118*, 13,347–13,360, doi:10.1002/2013JD020576.

Marcos, F. A., J. O. Wise, M. J. Kendra, N. J. Grossbard, and B. R. Bowman (2005), Detection of a long-term decrease in thermospheric neutral density, *Geophys. Res. Lett., 32*, L04103, doi:10.1029/2004GL021269.

Marsh, D. R., R. R. Garcia, D. E. Kinnison, B. A. Boville, F. Sassi, S. C. Solomon, and K. Matthes (2007), Modeling the whole atmosphere response to solar cycle changes in radiative and geomagnetic forcing, *J. Geophys. Res.*, *112*, D23306, doi:10.1029/2006JD008306.

Marsh, D. R., Mills, M. J., Kinnison, D. E., Lamarque, J.-F., Calvo, N., & Polvani, L. M. (2013). Climate change from 1850 to 2005 simulated in CESM1(WACCM), 73727391. *Journal of Climate*, *26*, 7372. https://doi.org/10.1175/JCLI-D-12-00558.1.

Neale, R., J. Richter, S. Park, P. Lauritzen, S. Vavrus, P. Rasch, and M. Zhang (2013), The mean climate of the Community Atmosphere Model (CAM4) in forced SST and fully coupled experiments, *J. Climate*, *26*, 5150–5168, doi:10.1175/JCLI-D-12-00236.1.

Qian, L., R. G. Roble, S. C. Solomon, and T. J. Kane (2006), Calculated and observed climate change in the thermosphere, and a prediction for solar cycle 24, *Geophys. Res. Lett.*, 33, L23705, doi:10.1029/2006GL027185.

Qian, L., J. Laštovička, R. G. Roble, and S. C. Solomon (2011), Progress in observations and simulations of global change in the upper atmosphere, *J. Geophys. Res.*, *116*, A00H03, doi:10.1029/2010JA016317.

Qian, L., D. Marsh, A. Merkel, S. C. Solomon, and R. G. Roble (2013), Effect of trends of middle atmosphere gases on the mesosphere and thermosphere, *J. Geophys. Res. Space Physics, 118*, doi:10.1002/jgra.50354.

Qian, L., S. C. Solomon, and R. G. Roble (2014), Secular changes in the thermosphere and ionosphere between two quiet Sun periods, *J. Geophys. Res. Space Physics*, *119*, doi:10.1002/2013JA019438.

Qian, L., A. G. Burns, S. C. Solomon, and W. Wang (2017), Carbon dioxide trends in the mesosphere and lower thermopshere, *J. Geophys. Res. Space Physics*, *122*, 4474, doi:1002/2016JA023825.

Randel, W. J., Polvani, L., Wu, F., Kinnison, D. E., Zou, C.-Z., and Mears, C. (2017), Troposphere-stratosphere temperaturetrends derived from satellite data compared with ensemble simulations from WACCM, *J. of Geophy. Res. Atmospheres*, *122*, doi:10.1002/2017JD027158.

Richmond, A. D., E. C. Ridley, and R. G. Roble (1992), A thermosphere/ionosphere general circulation model with coupled electrodynamics, *Geophys. Res. Lett.*, *19*, 601.

Rishbeth, H. and R. G. Roble (1992), Cooling of the upper atmosphere by enhanced greenhouse gases - modelling of thermospheric and ionospheric effects, *Planet. Space Sci.*, *40*, 1011, doi:10.1016/0032-0633(92)90141-A.

Roble, R. G., E. C. Ridley, A. D. Richmond, R. E. Dickinson (1988), A coupled thermosphere/ionosphere general circulation model, *Geophys. Res. Lett.*, *15*, 1325.

Roble, R. G., and R. E. Dickinson (1989), How will changes in carbon dioxide and methane modify the mean structure of the mesosphere and thermosphere? *Geophys. Res. Lett.*, *16*, 1144-1441.

Roble, R. G., and E. C. Ridley (1994), A thermosphere-ionosphere-mesosphere-electrodynamics general circulation model (TIME-GCM): Equinox solar cycle minimum simulations (30-500 km), *Geophys. Res. Lett., 21*, 417-420.

Saunders, A., H. Lewis, and G. Swinerd (2011), Further evidence of long-term thermospheric density change using a new method of satellite ballistic coefficient estimation, *J. Geophys. Res.*, *116*, A00H10, doi:10.1029/2010JA016358.

Solomon, S. C., and L. Qian (2005), Solar extreme-ultraviolet irradiance for general circulation models, *J. Geophys. Res.*, *110*, A10306, doi:10.1029/2005JA011160.

Solomon, S. C., T. N. Woods, L. V. Didkovsky, J. T. Emmert, and L. Qian (2010), Anomalously low solar extreme-ultraviolet irradiance and thermospheric density during solar minimum, *Geophys. Res. Lett.*, *37*, L16103, doi:10.1029/2010GL044468.

Solomon, S. C., L. Qian, L. V. Didkovsky, R. A. Viereck, and T. N. Woods (2011), Causes of low thermospheric density during the 2007–2009 solar minimum, *J. Geophys. Res.*, *116*, A00H07, doi:10.1029/2011JA016508.

Solomon, S. C., L. Qian, and A. G. Burns (2013), The Anomalous Ionosphere Between Solar Cycles 23 and 24, *J. Geophys. Res. Space Physics*, *118*, 6524, doi:10.1002/jgra.50561.

Solomon, S. C., L. Qian, and R. G. Roble (2015), New 3D simulations of climate change in the thermosphere, *J. Geophys. Res. Space Physics*, *120*, 2183, doi:10.1002/2014JA020886.

Zhang, S.-R., J. M. Holt, and J. Kurdzo (2011), Millstone Hill ISR observations of upper atmospheric long-term changes: Height dependency, *J. Geophys. Res., 116*, A00H05, doi:10.1029/2010JA016414.

Zhang, S.-R., and J. M. Holt (2013), Long-term ionospheric cooling: Dependency on local time, season, solar activity, and geomagnetic activity, *J. Geophys. Res. Space Physics, 118*, doi:10.1002/jgra.50306.

Zhang, S.-R., J. M. Holt, P. J. Erickson, L. P. Goncharenko, M. J. Nicolls, M. McCready, and J. Kelly (2016), Ionospheric ion temperature climate and upper atmospheric long term cooling, *J. Geophys. Res. Space Phys.*, *121*, 8951–8968, doi:10.1002/2016JA022971.

Table 1. Model inputs and Key Results

Inputs	*1972–1976*	*2001–2005*	*Change per decade*
$\langle CO_2 \rangle$ at surface	330 ppmv	375 ppmv	+16 ppmv
$\langle CH_4 \rangle$ at surface	1.44 ppmv	1.74 ppmv	+0.1 ppmv
<CFC11 + CFC12> at surface	0.29 ppbv	0.79 ppbv	+0.2 ppbv
$F_{10.7}$ index	70	70	0
K_p index	0.3	0.3	0
Results	*1972–1976*	*2001–2005*	*Change per decade*
$\langle T \rangle$ at surface	287.8 K	288.4 K	+0.2 K
$\langle T \rangle$ at 10 km (266 hPa)	225.8 K	226.9 K	+0.4 K
$\langle T \rangle$ at tropopause	204.2 K	204.5 K	+0.1 K
$\langle T \rangle$ at stratopause	262.9 K	259.6 K	-1.1 K
$\langle T \rangle$ at mesopause	193.1 K	191.0 K	-0.7 K
$\langle T \rangle$ at 400 km	697.9 K	689.9 K	-2.8 K
$\langle \rho \rangle$ at 400 km (mass density)	0.584 ng m^{-3}	0.518 ng m^{-3}	-3.9 %
$\langle NmF_2 \rangle$ (peak ion density)	1.78 x 10^5 cm^{-3}	1.71 x 10^5 cm^{-3}	-1.2 %
$\langle hmF_2 \rangle$ (height of peak)	261.5 km	257.8 km	-1.3 km
$\langle T_i \rangle$ at hmF_2 (ion temperature)	712.8 K	704.9 K	-2.7 K
Other Results for $\langle \rho \rangle$ *at 400 km: Observations*	*Comments*		*Change per decade*
Keating et al. (2000)	Low solar activity only		-5.0±1.4 %
Marcos et al. (2005)	Average solar activity		-1.7 to -2.4 %
Emmert et al. (2008)	For low solar activity		-5.5±1.4 %
Saunders et al. (2011)	For low-to-moderate solar activity		-7.2 %
Emmert et al. (2015)	For all solar activity levels		-3.0±1.0 %
Other Results for $\langle \rho \rangle$ *at 400 km: Models*	*Comments*		*Change per decade*
Roble & Dickinson (1989)	Low-to-moderate solar activity*		~ -3 %
Rishbeth & Roble (1992)	Low-to-moderate solar activity*		~ -2 %
Qian et al. (2006)	For low solar activity		-2.5 %
Akmaev et al. (2000, 2006)	At ~200 km altitude		-3 to -5 %
Solomon et al. (2015)	For low solar activity		-4.9 %
This Work	Low solar activity only		-3.9 %

*estimated from doubling scenario

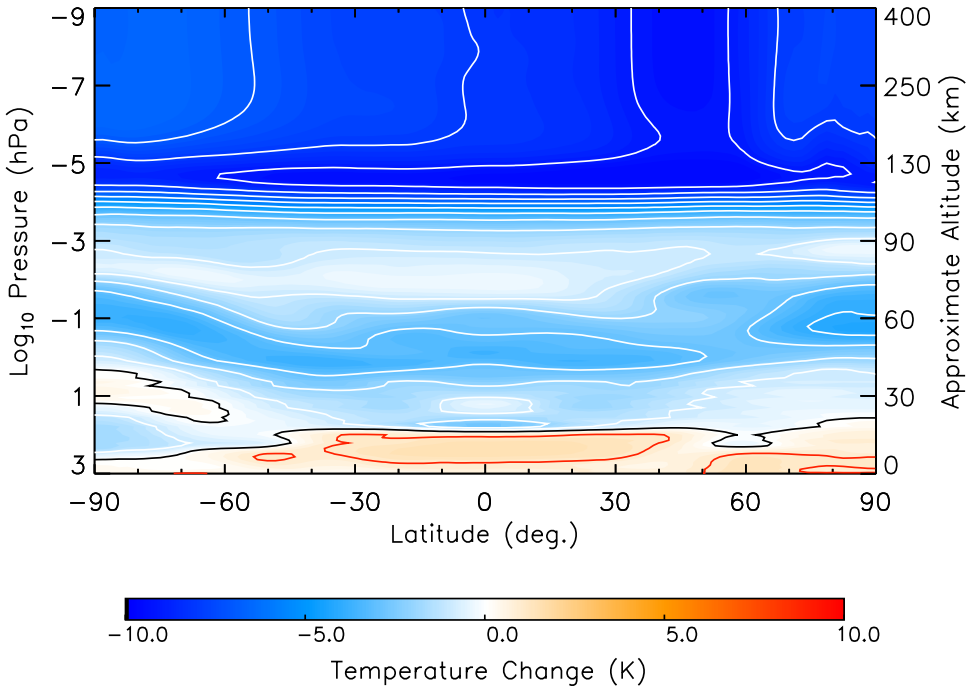

488

489 **Figure 1.** Model calculations of the zonal mean annual mean changes in temperature under low
490 solar activity conditions, as a function of latitude and pressure, for the 29-year simulation period
491 between five-year ensembes (1972–1976 to 2001–2005). Negative contours, ranging from -9 to -
492 1 K, with a 1 K interval, are shown in white; positive contours, at +1 and +2 K, are shown in red.
493 The zero-change line is shown in black.

494

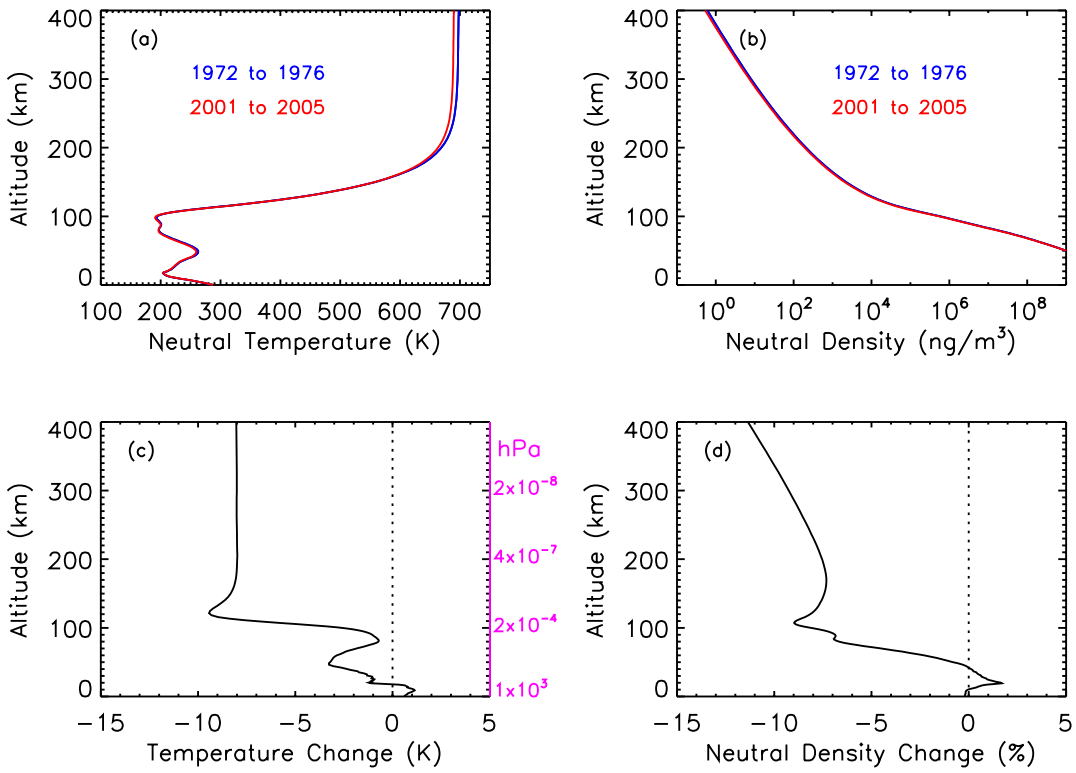

Figure 2. Model calculations of the modeled global mean annual mean changes, under low solar activity conditions, over the 29-year period between five-year ensembles (1972–1976 to 2001–2005), with CO_2 levels at the surface increasing from 330 to 373 ppmv. (a) Temperature profiles as a function of altitude. Blue: 1972–1976 (T_1). Red: 2001–2005 (T_2). (b) Neutral mass density as a function of altitude. Blue: 1972–1976 (n_1). Red: 2001–2005 (n_2). (c) Temperature change as a function of pressure, T_2-T_1. (d) Neutral number density percent change as a function of altitude, $100(n_2/n_1\text{-}1)$.

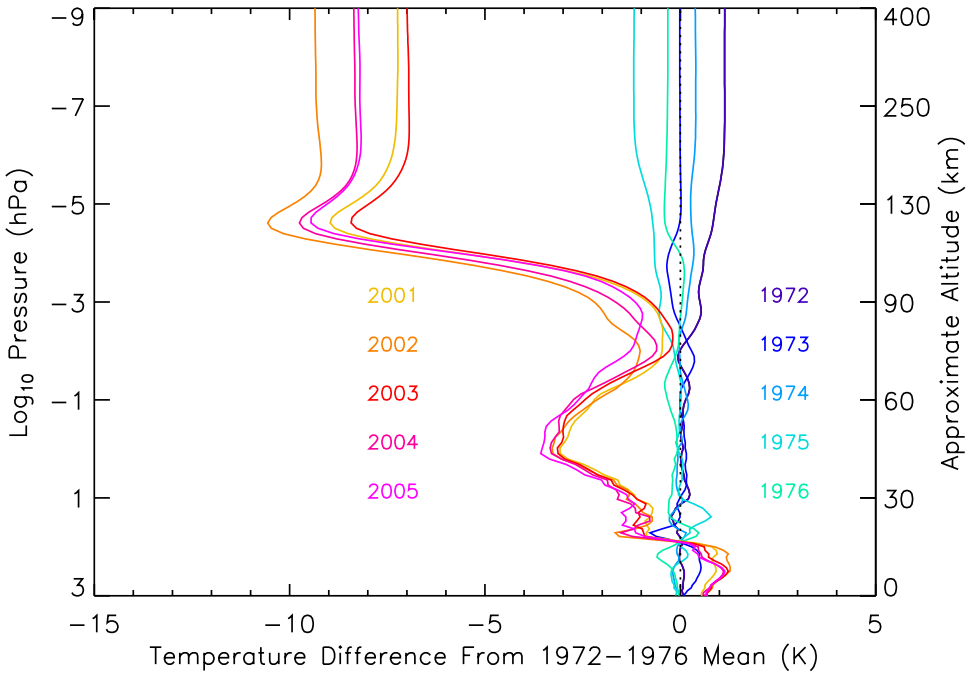

504

505 **Figure 3.** Interannual variability of global mean annual mean temperatures under constant low
506 solar and geomagnetic activity conditions. Temperature difference from mean of 1972 to 1976
507 simulations, as labeled.

508

Figure 1.

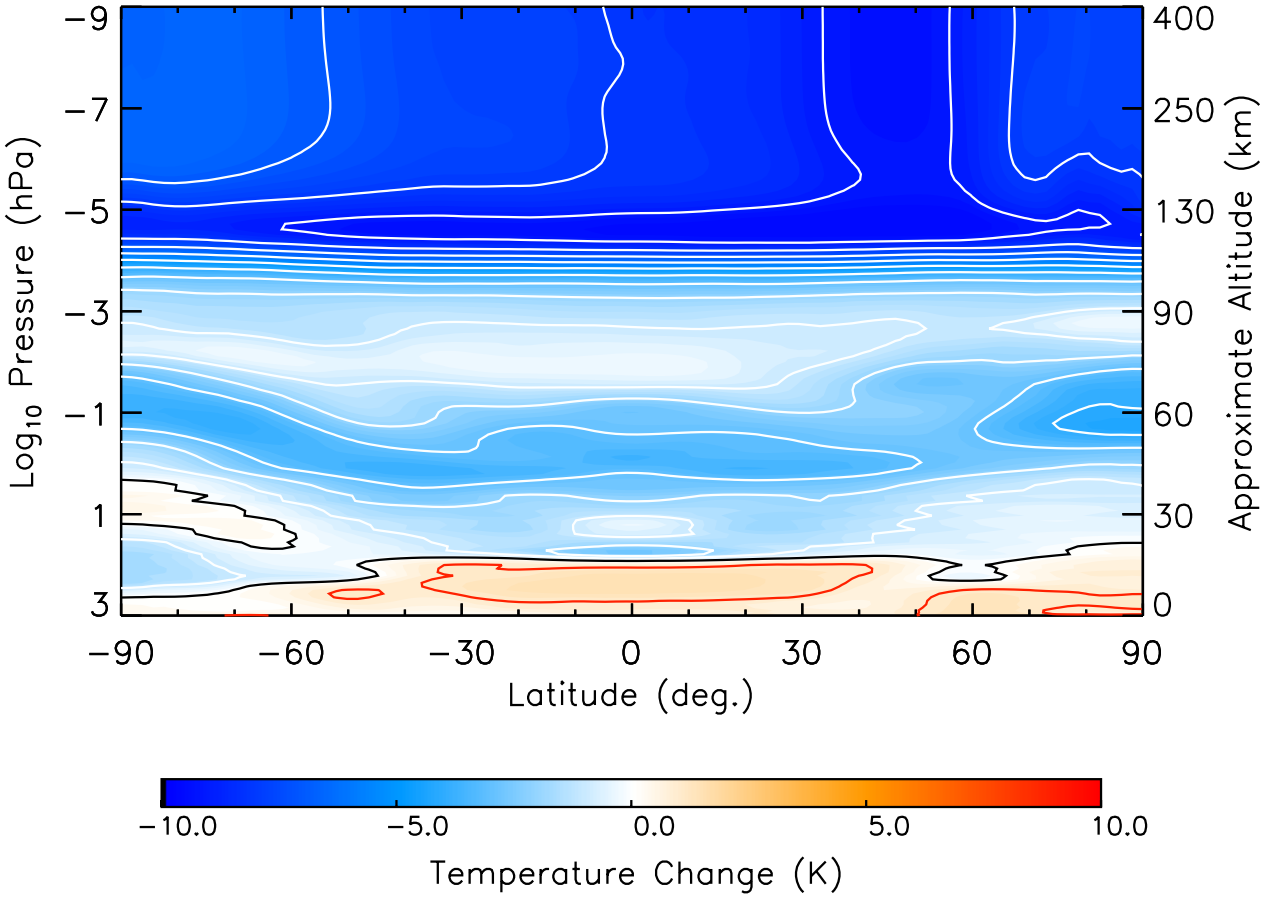
−9
−7
−5
−3
−1
1
3
Log10 Pressure (hPa)
400
250
130
90
60
30
0
Approximate Altitude (km)
−90
−60
−30
0
30
60
90
Latitude (deg.)
−10.0
−5.0
0.0
5.0
10.0
Temperature Change (K)

Figure 2.

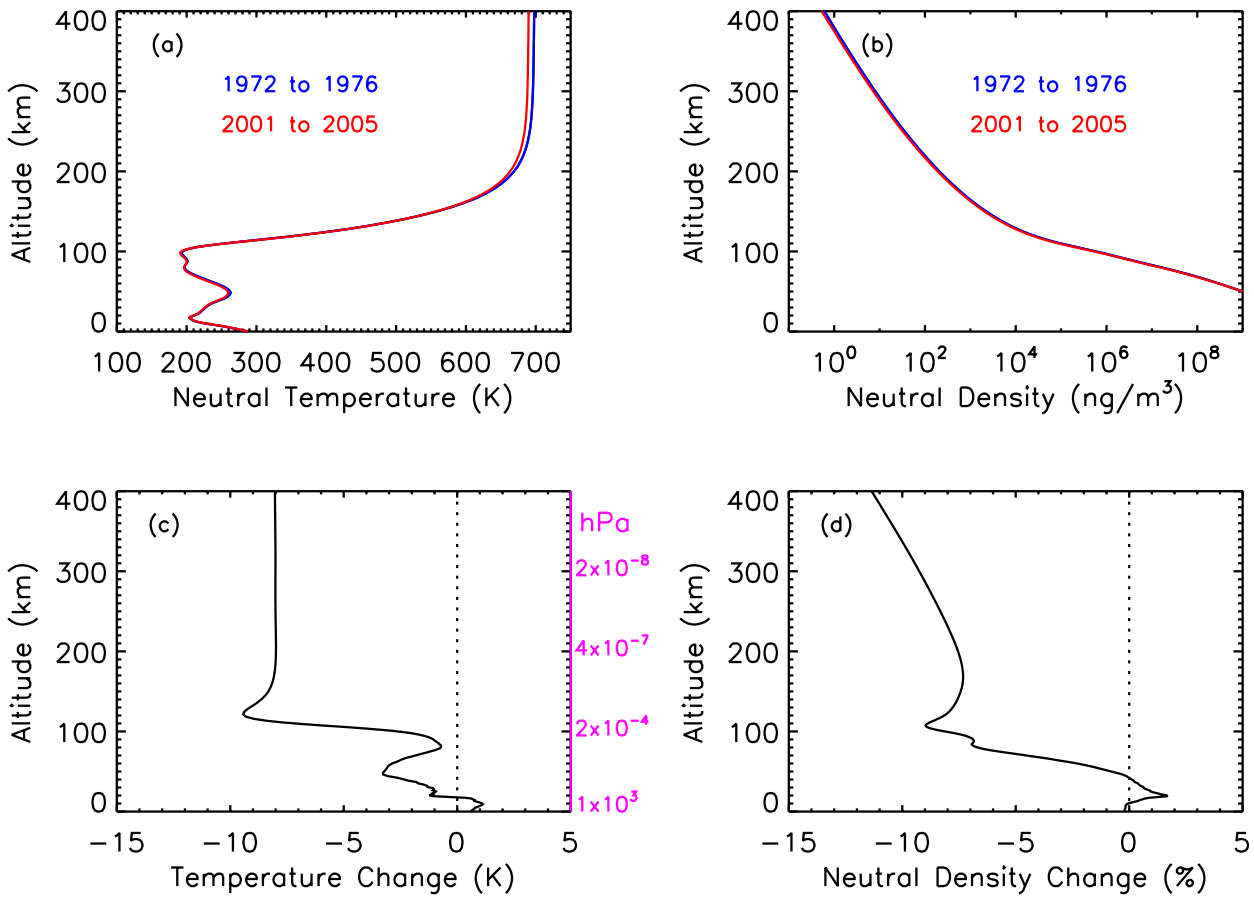
(a)
1972 to 1976
2001 to 2005
Altitude (km)
Neutral Temperature (K)
(b)
Neutral Density (ng/m3)
(c)
hPa
Temperature Change (K)
(d)
Neutral Density Change (%)

Figure 3.

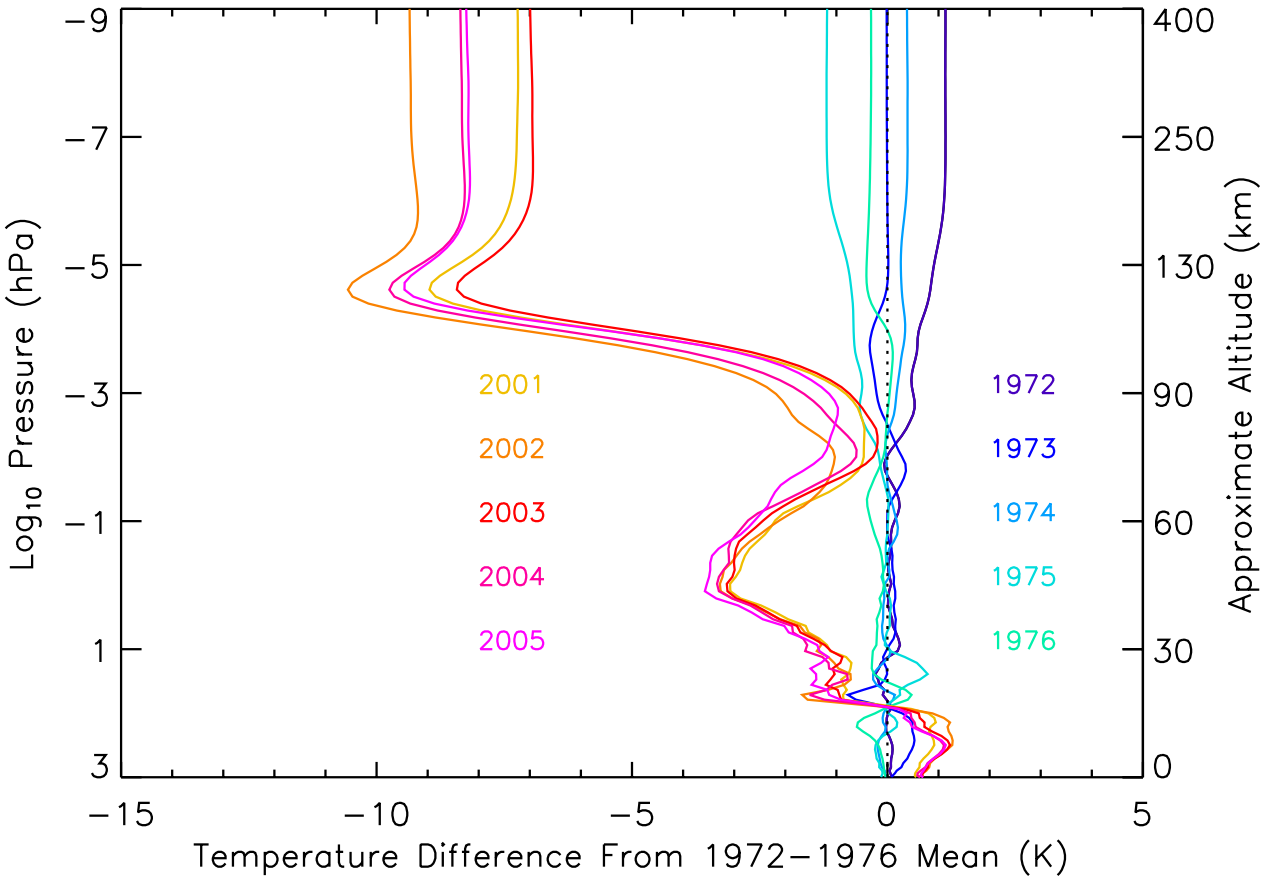
−9
−7
−5
−3
−1
1
3
Log10 Pressure (hPa)
400
250
130
90
60
30
0
Approximate Altitude (km)
2001
2002
2003
2004
2005
1972
1973
1974
1975
1976
−15
−10
−5
0
5
Temperature Difference From 1972−1976 Mean (K)